

## The notochord of hagfish *Myxine glutinosa*: visco-elastic properties and mechanical functions during steady swimming

John H. Long, Jr<sup>1,2,\*</sup>, Magdalena Koob-Emunds<sup>1,3</sup>, Benjamin Sinwell<sup>1,2</sup> and Thomas J. Koob<sup>1,3</sup>

<sup>1</sup>Mount Desert Island Biological Laboratory, Salsbury Cove, Maine, 04672, USA, <sup>2</sup>Department of Biology, Vassar College, Poughkeepsie, New York, 12604, USA and <sup>3</sup>Division of Skeletal Biology, Shriners Hospital for Children, Tampa, Florida, 33612, USA

\*Author for correspondence (e-mail: jolong@vassar.edu)

Accepted 9 September 2002

### Summary

To determine the possible locomotor functions of the hagfish notochord, we measured its flexural stiffness  $EI$  ( $\text{Nm}^{-2}$ ) and flexural damping  $C$  ( $\text{kg m}^3 \text{s}^{-1}$ ), under *in vitro* conditions that mimicked the body curvature and bending frequency measured during steady undulatory swimming. To assess the notochord's contribution to the mechanical behavior of the whole body, we also measured  $EI$  and  $C$  of the whole body, the body with skin removed, and the notochord with the outer fibrous sheath removed. When subjected to dynamic bending at angular frequencies from  $\pi$  to  $6\pi \text{ rad s}^{-1}$  and midline curvatures from 11 to  $40 \text{ m}^{-1}$ , 1 cm *in situ* body segments ( $N=4$ ), located at an axial position of 37% of the body length, showed significant changes in  $EI$ ,  $C$ , the Young's modulus or material stiffness ( $E$ , MPa), the net work to bend the body over a cycle ( $W$ , J) and resilience ( $R$ , % energy return). When skin, muscles and the outer fibrous sheath of the notochord were removed sequentially, each structural reduction yielded significant changes in mechanical properties:  $C$  decreased when the skin was removed,  $E$  increased when the muscles were removed, and  $EI$  and  $R$  decreased when the outer fibrous sheath was removed.

Although occupying only a small portion of the cross-sectional area, the notochord provides the body with 75% of its total  $EI$  and 80% of total  $C$ , by virtue of its high  $E$ , ranging from 4 to 8 MPa, which is an order of magnitude greater than that of the whole body. Thus, as the body's primary source of  $EI$  and  $C$ , the notochord determines the passive (i.e. internal, non-muscular) mechanical behavior of the swimming hagfish.  $EI$  and  $C$  covary inversely and non-linearly such that as  $C$  increases,  $EI$  decreases. However, the bending moments  $M$  ( $\text{Nm}$ ) produced by each property increase proportionally, and the ratio of stiffness to damping moments, also known as the amplification ratio at resonance, is nearly invariant (approximately 7) with changes in driving frequency. If the body operates in life at or near resonance, the variables  $EI$  and  $C$  interact over a range of swimming speeds to produce passive mechanical stability.

Key words: notochord, backbone, axial skeleton, hagfish, swimming, bending, damping, stiffness, flexural stiffness, kinematics, visco-elastic properties, *Myxine glutinosa*.

### Introduction

Chordates have evolved an unique hydrostatic axial skeleton, the notochord, that is present in all taxa of that phylum early in development; it is retained in the adults of some taxa and modified by vertebral elements in others (Gee, 1996). Notochords are hypothesized to have evolved to stiffen the body (Goodrich, 1930) and to prevent body compression during muscle activation (Clark, 1964). In addition, notochords may adjust function by means of dynamically variable mechanical properties (Long et al., 1998). Our goal was to determine the notochord's locomotor functions by measuring its mechanical properties and behavior, relative to those of the intact body, under conditions that mimic those of steady undulatory swimming.

We chose to study Atlantic hagfish *Myxine glutinosa* because (1) as adults they retain a notochord without

vertebral elements (Cole, 1905), (2) they are active undulatory swimmers (Adams, 1960; Martini et al., 1997), bending their notochord dynamically, and (3) they belong to the living sister taxon (Myxiniformes) to vertebrates and thus provide information to assist in phylogenetic reconstruction of the ancestral craniate notochord. The notochord of hagfish has also attracted considerable attention because of its unusual biochemical, molecular and biomechanical properties (Koob et al., 1994; Kielstein et al., 1996; Long et al., 1998; Welsch et al., 1998). In a preliminary biomechanical study (Long et al., 1998), the visco-elastic properties of the Atlantic hagfish's notochord were compared to those of the whole body, and more than half of the whole body's passive flexural stiffness and damping were attributed to the notochord alone.

Flexural stiffness and damping are keys to understanding the dynamic functions of notochords. When vibrations, such as a fish's undulatory body waves, are driven at a bending frequency  $\omega$  ( $\text{rad s}^{-1}$ ) lower than the structure's resonant or natural frequency, bending motion and internal stress are dominated by the structure's flexural stiffness,  $EI$  (in  $\text{N m}^2$ ). As  $\omega$  approaches and then equals the natural frequency, flexural stiffness and the mass moment of inertia  $I_m$  ( $\text{kg m}^2$ ), balance, causing bending motion and internal stress to increase rapidly and catastrophically unless sufficient damping forces are present (Den Hartog, 1956; Denny, 1988). This amplification is expressed as the ratio of the maximal stiffness moment  $EI\kappa_0$ , to the maximal applied moment  $M_0$  (N m) driving the vibrations (modified from Denny, 1988):

$$\frac{EI\kappa_0}{M_0} = \frac{EI}{\sqrt{(EI - I_m l \omega^2)^2 + (C\omega)^2}}, \quad (1)$$

where  $\kappa_0$  is the amplitude of curvature ( $\text{m}^{-1}$ ),  $C$  is the flexural damping ( $\text{kg m}^3 \text{s}^{-1}$ ) and  $l$  is the length of the structure (m). This ratio is a relative measure of the amplification of the dynamic moments experienced by the oscillating structure, with values above 1 indicating amplification and those below indicating attenuation (Denny, 1988).

To examine their relative importance in swimming and bending hagfish, we measured  $EI$  and  $C$  *in situ* at physiologically relevant frequencies and curvatures using a custom-built, dynamic bending machine (Long, 1998). We determined the natural physiological parameters for the bending tests from kinematic analysis of steadily swimming hagfish. To understand the contributions of specific structures to the overall visco-elastic properties of the body, we compared, in dead hagfish, the properties of the whole body with those of the skinless body, the intact notochord, and the core of the notochord. Specifically, we asked two questions. (1) Over the range of lateral bending motions seen during swimming, what are the body's passive visco-elastic properties? (2) Compared to skin and muscle, does the notochord contribute substantially during swimming to the body's passive mechanical functions?

## Materials and methods

### Animals

Hagfish *Myxine glutinosa* L. were purchased from a commercial supplier (Huntsman Marine Laboratory, New Brunswick, Canada), who caught the specimens in baited traps in the Bay of Fundy. At Mount Desert Island Biological Laboratory, Salsbury Cove, Maine, hagfish were kept in circular 400 l tanks with running seawater at 10–12°C. 16 post-absorptive hagfish were used, 8 in swimming trials and 8 in bending experiments (for lengths and masses, see Table 1). Following swimming trials and prior to bending experiments, animals were killed with an overdose of propylene phenoxetol. During testing, tissues were continually bathed in chilled hagfish Ringer solution (Riegel, 1978).

### Kinematic analysis of steady swimming

From a distance of 3 m, we simultaneously videotaped (SVHS format, 60 images  $\text{s}^{-1}$ , shutter speed 0.001 s; Hitachi Model KP-M1U) lateral and dorsal views of swimming hagfish through transparent walls and by the use of a front-surface mirror (Edmund Scientific) mounted at 45° above a still-water circuit (2 m straight sections connected by turns of 1 m radius). After gentle manual prodding, hagfish swam readily at speeds of their own volition. We used only those trials in which fish swam (i) without touching the walls and (ii) steadily, as defined by linear regression ( $r^2 > 0.98$  for one tailbeat cycle) of axial displacement against time of body point 11 (Fig. 1D; see below). By these criteria, 23 trials were selected (3 trials from 7 fish and 2 trials from 1 fish). Body point 11, the position that corresponds to the portion of the body bent during dynamic tests (0.37  $L$  from rostrum, where  $L$  is body length), was chosen because, as the propulsive wave of bending propagates from

Table 1. Morphometrics of hagfish and test sections used in each experimental group

Hagfish	Body mass (kg)	Body length $L_b$ (m)	Test section length $l$ (m)
Group 1: Swimming trials			
1	0.034	0.284	0.009
2	0.036	0.329	0.011
3	0.038	0.298	0.010
4	0.039	0.314	0.010
5	0.040	0.315	0.011
6	0.042	0.298	0.010
7	0.046	0.330	0.011
8	0.049	0.324	0.011
Mean±S.D.	0.041±0.0050	0.311±0.0167	0.010±0.0006
<i>t</i> -test*	A	C	F
Group 2: Structural treatments 1–3			
9	0.039	0.377	0.012
10	0.041	0.380	0.010
11	0.045	0.375	0.010
12	0.058	0.385	0.011
Mean±S.D.	0.046±0.0083	0.379±0.0044	0.011±0.0010
<i>t</i> -test	A, B	D	F
Group 3: Structural treatment 4			
13	0.070	0.415	0.006
14	0.069	0.427	0.003
15	0.044	0.415	0.004
16	0.065	0.425	0.004
Mean±S.D.	0.062±0.0122	0.0421±0.0064	0.004±0.0013
<i>t</i> -test	B	E	G

*t*-tests were for two-tailed distributions with heteroscedastic variances conducted on the three pairwise comparisons of the three group samples. The same letter indicates that there was no detectable difference in the means of the groups ( $P > 0.05$ ).

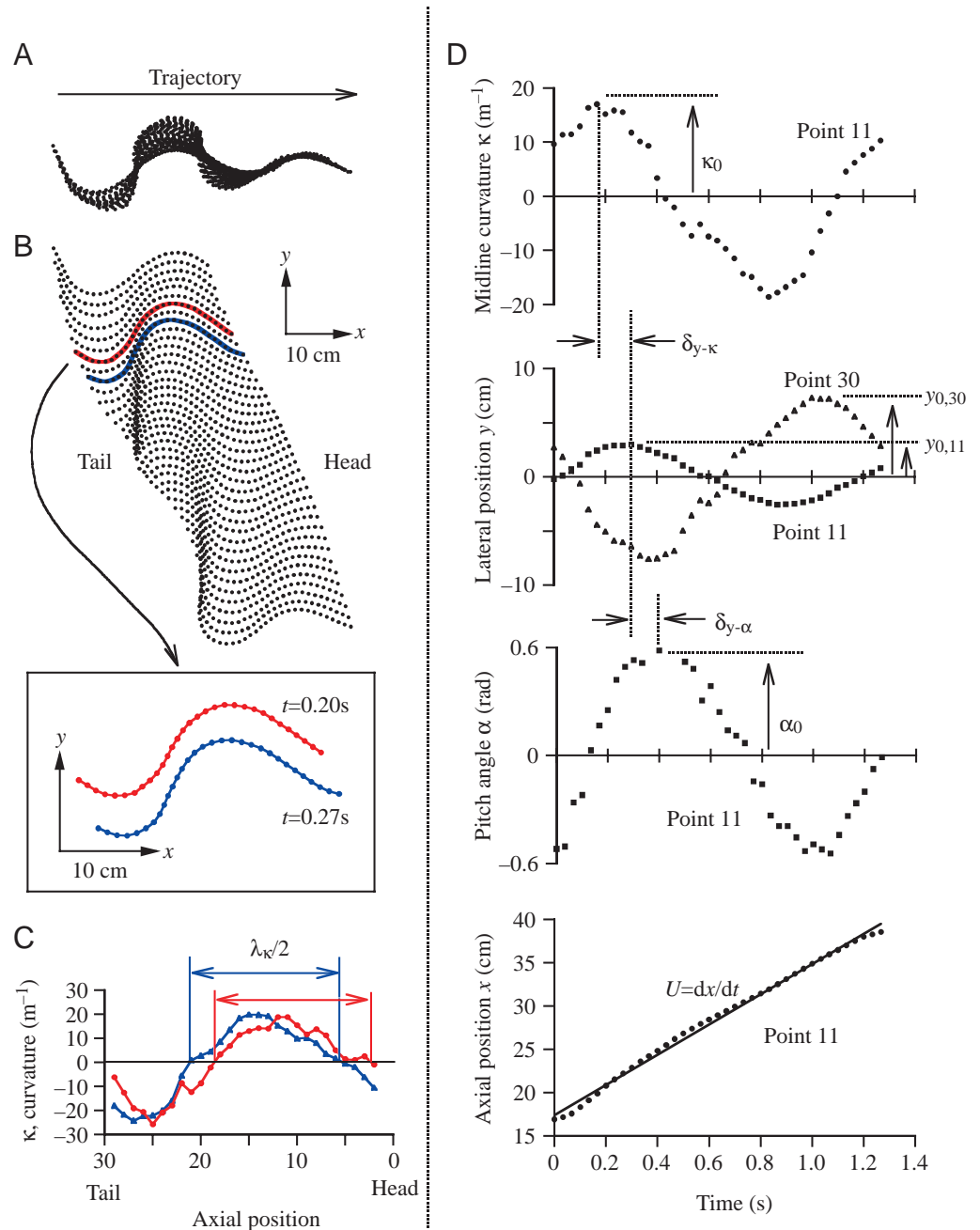
See Materials and methods and Fig. 2 for an explanation of the structural treatment categories.

head to tail, it was the first point to contain a nearly complete half-wave of curvature (see Fig. 1B; Table 3). With a complete half-wave on both sides of this position, anterior and posterior bending moments are roughly balanced and can thus be imposed as such on experimental sections (see below). Since we did not measure kinematics or mechanical properties at other axial positions, extrapolations should be made cautiously.

From the videotape of each steady swimming trial, we manually digitized the dorsal midline of the hagfish for a complete tailbeat cycle by overlaying (Digital Vision, Inc. model TelevEyes Pro) a computer-generated  $x$ - $y$  coordinate grid (National Institutes of Health version 1.46 on an Apple

Corp. model Macintosh G3) onto a digitally paused video image (Sony Model MD 9500 MDR). 20 points along the midline, starting at the tip of the rostrum and ending at the tip of the tail, were selected sequentially at points equidistant from the lateral edges of the body. Each set of 20 digitized points was fitted with a smooth function using a custom compound-spline software package (Jayne and Lauder, 1993). The spline function was used to generate a segmented midline of 31 points (numbered 0–30), 30 segments of equal length, and 29 joints (Fig. 1A,B). From this reconstructed midline we measured the  $x$  and  $y$  position of each point and each joint's flexion, the angular deviation  $\theta$  (in rad) of the joint (Fig. 1D) from a straight line (Jayne and Lauder, 1993). Because the entire

Fig. 1. Swimming motions and kinematic variables. (A) A swimming hagfish ( $TL$  31.5 cm), as represented by overlaid, reconstructed midlines (31 points each) from one tailbeat cycle. (B) Midlines displaced vertically (time descends) to show curvature and forward progression ( $17.5 \text{ cm s}^{-1}$ ). Inset: Midlines at times 0.20 s and 0.27 s are magnified to show placement of points 0–30 evenly along the midline. (C) The curvature half-wave length,  $\lambda_{\kappa}/2$  ( $L$ ), is the axial distance along the midline from the points of 0 to 0 midline curvature,  $\kappa$  ( $\text{m}^{-1}$ ). (D) Other kinematic variables include amplitude of the midline curvature,  $\kappa_0$ , amplitude of the lateral displacement of body points 11,  $y_{0,11}$ , and 30,  $y_{0,30}$ , amplitude of the pitch angle,  $\alpha_0$ . The phase lags  $\delta_{y-\kappa}$  and  $\delta_{y-\alpha}$ , are the differences in time, as a fraction of the normalized tailbeat period ( $T$ ), between maximal  $y$  and maximal  $\kappa$  and  $\alpha$ , respectively.



section was bending not as a hinge, as implied by  $\theta$ , but as a small cantilevered beam, we converted  $\theta$  to midline curvature  $\kappa$  (in  $\text{m}^{-1}$ ), using the following formula, which was derived from trigonometry assuming uniform curvature along the small length  $l$ , of the body segment:

$$\kappa = \frac{2\sin\left(\frac{\theta_0}{2}\right)}{l}. \quad (2)$$

From the motion of the reconstructed midline, a number of other kinematic variables were measured (Fig. 1). For the purpose of designing physiologically relevant bending experiments, of primary importance were the amplitude of the midline curvature  $\kappa_0$ , and the tailbeat or undulatory frequency  $\omega$  ( $\text{rad s}^{-1}$ ). Tailbeat frequency is measured as the quotient of  $2\pi$  (rad) and the tailbeat period (s), which is the time required by body point 30, the tail tip, to twice achieve values of zero lateral displacement following an initial zero displacement (Fig. 1D). Other kinematic variables measured included lateral amplitude ('heave') of body point 11,  $y_{0,11}$ , lateral amplitude of the tail tip (point 30),  $y_{0,30}$ , and amplitude of the pitch angle  $\alpha_0$  of the body segment between midline points 10 and 11 (Fig. 1D). The instantaneous pitch angle  $\alpha$  (rad) is defined as the orientation of the segment relative to the direction of the freestream flow (Vogel, 1994), which is approximately the  $x$ -axis or the axis of progression. The relative timings of maximal heave, flexion and pitch at midline point 11 were measured as the phase lag (fraction of a tailbeat period  $T$ ) between the time of maximal heave and flexion  $\delta_{y-\kappa}$ , and between the time of maximal heave and pitch  $\delta_{y-\alpha}$ . For positive values of phase lag the maximal heave occurs later in the tailbeat cycle than either the flexion or pitch maxima.

Using a technique modified from McHenry (2001), we defined the curvature half-wave length,  $\lambda_{\kappa}/2$ , as the distance (as a proportion of normalized body length  $L$ ) along the body axis from zero to zero  $\kappa$ , i.e. from inflection point to inflection point;  $\lambda_{\kappa}/2$  was measured on the body when the half-wave included body point 11, the position that corresponds to the portion of the body bent during dynamic tests ( $0.37L$  from rostrum). Thus, the reported value of  $\lambda_{\kappa}/2$  for each trial is the average of all the instantaneous values of  $\lambda_{\kappa}/2$  (Fig. 1C). The curvature half-wave is roughly analogous to the so-called propulsive wave or half-wave, measured as the distance along the axis of progression (roughly the  $x$ -axis in Fig. 1) between midline nodes, as determined by a variety of methods (for caveats and a review, see Long and Nipper, 1996). The  $\lambda_{\kappa}/2$  value has the advantage over the standard propulsive wavelength of being independent of (i) the estimation of the axis of progression, (ii) the requirement of left-right symmetry in body bending, (iii) the determination and subtraction of average body velocity from the midline points and (iv) the lateral position of the tail.

To determine which variables predicted length-specific swimming speed,  $U_L$  (in  $L s^{-1}$ ), we ran the following general linear model using the statistical software JMP (SAS Institute,

Inc., version 3.0). Because the 23 swimming trials were from eight individuals, we included individual, IND, as a randomized-block effect:

$$U_L = c + \text{IND} + \kappa_0 + \omega + y_{0,11} + y_{0,30} + \alpha_0 + \delta_{y-\alpha} + \delta_{y-\kappa} + \frac{\lambda_{\kappa}}{2}, \quad (3)$$

where  $c$  is a constant. In addition, we used univariate linear regressions to test if  $\kappa_0$  and  $\omega$  were, individually, significant predictors of the remaining kinematic variables.

#### Dynamic bending tests

In order to determine the flexural stiffness  $EI$  and the flexural damping  $C$  of the hagfish body axis, we used the methodology and machinery of Long (1998). To produce sinusoidal cantilever bending, the caudal side of a small portion of the intact body was clamped on a stationary strain gauge and the cranial side was clamped onto a motor-driven linkage that applied a bending couple of varying curvature amplitude  $\kappa_0$  and frequency  $\omega$ . The strain gauge measured the bending moment  $M$  transmitted through the body section. Dynamic  $M$  signals produced by the strain gauge (two 120  $\Omega$  foil gauges; Omega Engineering) were excited and amplified by a high-frequency (40 kHz response time) bridge amplifier (Omega Engineering model DMD-520) and were digitally recorded at 1000 Hz (National Instruments model NB-MIO16E analog-to-digital converter). Simultaneously and in the same file, we digitally sampled the  $\kappa$ , which was determined using a rotary variable differential transducer (Schaevitz model R30D) mounted colinear with the bending couple input linkage; it measured  $\theta$  that we converted to  $\kappa$  using Equation 2.

We determined  $EI$  and  $C$  for a given experimental trial (fixed  $\kappa$  and  $\omega$ ) using the equation of motion for a single-degree-of-freedom system (see Den Hartog, 1956):

$$M_0 \sin(\omega t) = EI \kappa_0 \sin(\omega t - \delta) + C \omega \kappa_0 \cos(\omega t - \delta), \quad (4)$$

where the term  $\kappa_0 \sin(\omega t - \delta)$  is the curvature as a function of time  $t$ ,  $\omega \kappa_0 \cos(\omega t - \delta)$  is the rate of change of curvature with respect to time, and  $\delta$  is the phase lag (rad) between the maxima of  $\kappa$  and  $M$ . Note that inertia in the particular experimental apparatus is negligible and thus, for measuring  $EI$  and  $C$ , is ignored (Long, 1998). Because the  $EI$  and  $C$  terms are  $90^\circ$  out of phase, when the  $EI$  term is maximal the  $C$  term is zero. With the help of trigonometric identities, Equation 4 simplifies and can be rewritten:

$$EI = \frac{M_0 \cos \delta}{\kappa_0}. \quad (5)$$

Likewise, when  $EI$  is zero,  $C$  is maximal and thus Equation 4 simplifies and can be rewritten:

$$C = \frac{M_0 \sin \delta}{\omega \kappa_0}. \quad (6)$$

For a trial at a given  $\kappa_0$  and  $\omega$ , the measured  $C$  values were used to calculate the net flexural work  $W$  (J), used over a

complete cycle to bend the sample. The  $W$ , also known as the work to overcome damping  $C$ , was calculated as follows (see Den Hartog, 1956):

$$W = \pi C l \omega \kappa_0^2. \quad (7)$$

In addition,  $EI$  can be divided by  $I$ , the area moment of inertia ( $\text{m}^4$ ), in order to yield the apparent material stiffness  $E$  (in MPa), or Young's modulus. Since hagfish have a nearly circular cross-section (see Fig. 2),  $I$  is given as follows (Denny, 1988):

$$I = \frac{\pi}{4} r^4, \quad (8)$$

where  $r$  is the radius of the hagfish's cross-section. The resilience  $R$  (% energy return) of the test section was calculated as follows (Wainwright et al., 1976):

$$R = \frac{100}{e^{\pi \tan \delta}}. \quad (9)$$

Finally, to determine if these mechanical properties varied with changes in  $\kappa$  and  $\omega$ , we varied those parameters over a range ( $11\text{--}40 \text{ m}^{-1}$ ;  $\pi\text{--}6\pi \text{ rad s}^{-1}$ , respectively) that included

physiological values of midline curvature  $\kappa_0$  and undulatory frequency  $\omega$  (see Results).

To determine the relative influence of axial structures on  $EI$ ,  $E$ ,  $C$ ,  $W$  and  $R$ , we sequentially removed, by dissection, the skin, the lateral musculature, and the notochord's outer fibrous sheath (Fig. 2). The removal of the lateral musculature (change from the 'without skin' to 'notochord', structural treatment categories 2 and 3, respectively), significantly decreased mean width, area and  $I$  of the test sections (Fig. 2). Removal of the outer fibrous sheath (change from 'notochord' to 'core', structural treatment categories 3 and 4, respectively) significantly decreased the mean width of the test sections (Fig. 2A). While changes in morphometrics were not statistically detectable (although a consistent decreasing trend exists) between the 'intact' and 'skin-removed' categories (structural treatment categories 1 and 2, respectively), this change removes the subcutaneous blood sinus (Forster, 1997). The skin and the lateral musculature were removed while the hagfish body was clamped in the bending machine. In order to remove the outer fibrous sheath without damaging the core, we dissected the intact axial skeleton from the body, and then carefully

removed the outer fibrous sheath with a scalpel. Because the core was occasionally damaged in this process, we used the cores from different individuals than those used for the first three structural treatment categories.

The body and notochord were tested using section lengths,  $l$ , of  $0.004\text{--}0.010 \text{ m}$  long (Table 1), depending on the experimental treatment. The test section was centered at  $0.37L$ , the same position for which we measured kinematic features of swimming (see previous section). For structural treatment categories 1–3, only the test section was altered; the rest of the body was intact, attached, and unaltered. For structural treatment category 4, the entire notochordal core was kept intact. Prior to each test, the section was conditioned by undergoing at least 20 cycles of bending. Potential order effects (the potential for sample degradation over time to be correlated with serially

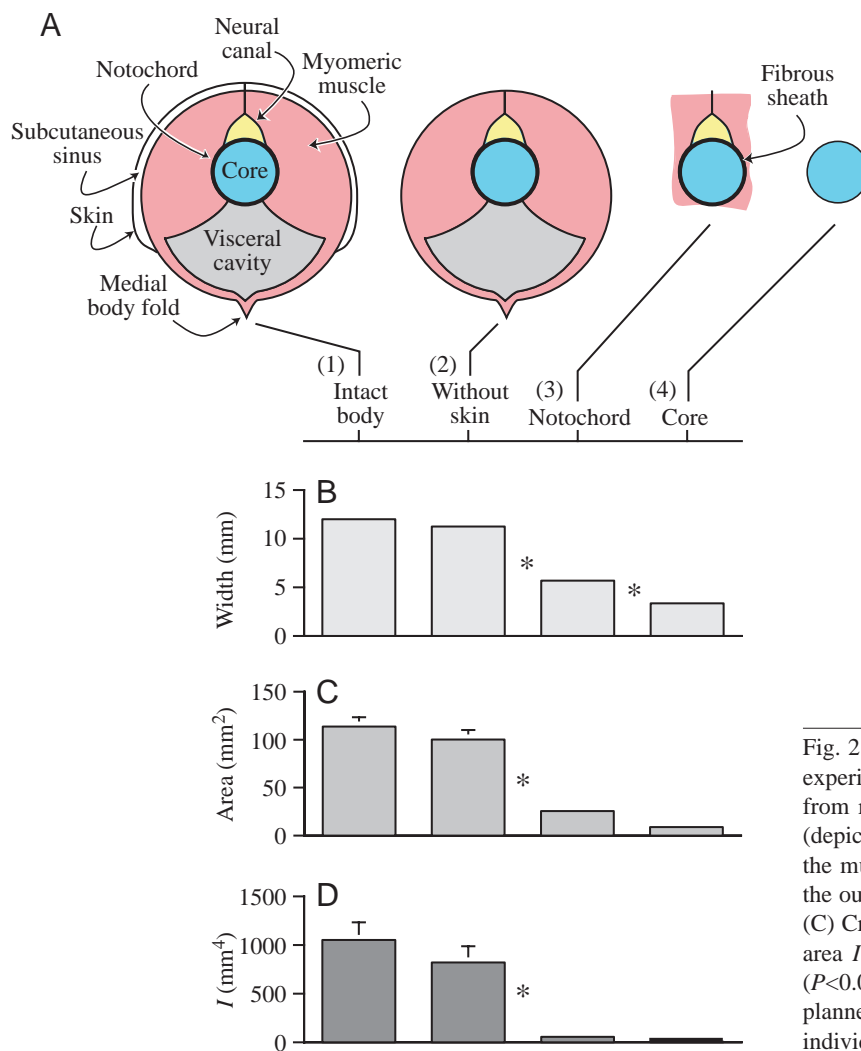


Fig. 2. Structural treatments 1–4 used in bending experiments. (A) Cross-sectional view of body axis at  $0.37L$  from rostrum. The body segment (1) was serially dissected (depicted from left to right) with the skin removed (2), then the muscle removed (leaving the notochord) (3), and finally the outer fibrous sheath removed (4). (B) Width of the body. (C) Cross-sectional area of the body. (D) Second moment of area  $I$  of the body. Asterisks denote significant differences ( $P < 0.05$ ) between adjacent means as determined using planned contrasts in a repeated-measures ANOVA ( $N = 8$  individual hagfish).

arranged tests) for structural treatments were unavoidable, given the need for sequential dissection and to minimize the number of animals used. Order effects were also possible for the tests within a structural treatment category, since tests proceeded from lowest frequency and amplitude to highest frequency and amplitude. To test the magnitude of the order effects, we repeated the first tests following the last; in no case did identical test conditions, separated by time and testing, reveal changes in  $E$  or  $C$  greater than 3%.

The notochordal core treatment confounded our statistical analysis in two ways. (1) In order to produce a detectable  $M$  signal with the small-diameter of the core, we increased the applied  $\kappa$  by reducing the length,  $l$ , of the test section. Since the range of  $\kappa$  values was, thus, higher than that used for structural treatment categories 1–3, we nested the factor  $\kappa$  within the factor ‘structural treatment’ TRT, which produced a single nested factor equivalent to the factor  $\kappa$  and the  $\kappa$  by TRT interaction term (Zar, 1996). (2) Cores were from individuals different from those in structural treatments categories 1–3, therefore we nested the factor individual, IND, within the  $\kappa$  and TRT factors. This produced a compound nested factor equivalent to the factor IND and the IND by  $\kappa$  by TRT interaction (Zar, 1996). The result was a mixed-model nested analysis of variance (ANOVA) with  $\omega$  and TRT as main effects:

$$(EI, E, C, W, \text{ or } R) = \omega + \text{TRT} + \omega \times \text{TRT} + \kappa[\text{TRT}] + \text{IND}[\text{TRT}, \kappa]. \quad (10)$$

To test for differences between adjacent levels of the factors  $\omega$  and TRT, we ran *a priori* contrasts. Analysis was conducted in JMP (SAS Institute, Inc., version 3.0).

## Results

### Swimming kinematics

In a still-water tank, hagfish swam steadily using undulatory body waves. The length-specific swimming speed  $U_L$ , was predicted by a single variable, the undulatory frequency  $\omega$ , which increased linearly with increasing  $U_L$  (Table 2, Fig. 3). In turn,  $\omega$  was inversely proportional to the tailbeat amplitude  $y_{0,30}$ , and was directly proportional to the phase lag between lateral displacement and curvature  $\delta_{y-\kappa}$  (Table 3, Fig. 3). The other kinematic variables were independent of  $U_L$  and  $\omega$ . In addition, while the amplitude of midline curvature,  $\kappa_0$ , was not a significant predictor of  $U_L$ , it was directly proportional to the amplitude of the pitch angle,  $\alpha_0$  and  $\delta_{y-\kappa}$ .

### Visco-elastic properties of the notochord and body

Overall, dynamic bending tests at  $0.37L$  revealed that the visco-elastic properties of the body varied significantly as functions of the bending frequency  $\omega$ , structural treatment TRT, the interaction of  $\omega$  and TRT, and individual IND, nested within TRT and curvature,  $\kappa$ ;  $\kappa$  nested within TRT was not a significant factor for any response variable. Specifically, with changes in  $\omega$ , flexural stiffness  $EI$ , flexural damping  $C$  and flexural work  $W$ , all varied significantly (Table 4). *A priori*

Table 2. Swimming speed  $U_L$  of hagfish as a function of the midline kinematic variables, determined by multiple regression

Independent variable (d.f.)	Sum of squares (s.s.)	F ratio	P
Individual (7)	0.0791	3.17	0.078
$\kappa_0$ (1)	0.0101	2.83	0.137
$\omega$ (1)	0.0387	10.82	<b>0.013</b>
$\lambda_{\kappa}/2$ (1)	0.0012	0.34	0.455
$y_{0,11}$ (1)	0.0022	0.62	0.455
$y_{0,30}$ (1)	0.0082	2.30	0.173
$\alpha_0$ (1)	0.0031	0.86	0.384
$\delta_{y-\alpha}$ (1)	0.0040	1.13	0.324
$\delta_{y-\kappa}$ (1)	0.0003	0.11	0.755
<hr/>			
Summary of fit	ANOVA	F ratio	P
$N=23$	Model s.s.=0.3985	7.44	
$r^2=0.941$ , adj. $r^2=0.814$	Error s.s.=0.0250		<b>0.006</b>
adj., adjusted.			
$P<0.05$ is significant and indicated as such in bold, $N=23$ .			
In a <i>post-hoc</i> univariate regression, $U_L=0.3178+0.0419\omega$ ( $r^2=0.460$ , adj. $r^2=0.434$ ; $P=0.0004$ ).			
See List of symbols for definitions of variables and units.			

Table 3. Kinematic variables correlated with undulatory frequency,  $\omega$ , and/or amplitude of midline curvature  $\kappa_0$  as determined by linear regression\*

Dependent variable	Equation	$r^2$	adj. $r^2$	P
Lateral tail amplitude	$y_{0,30}=0.2272-0.0086\omega$	0.255	0.220	<b>0.014</b>
Pitch angle amplitude	$\alpha_0=0.198+0.0189\kappa_0$	0.332	0.300	<b>0.004</b>
Phase lag, curvature	$\delta_{y-\kappa}=-0.0522+0.0118\omega$	0.242	0.206	<b>0.017</b>
Phase lag, curvature	$\delta_{y-\kappa}=-0.0736+0.0074\kappa_0$	0.190	0.151	<b>0.038</b>
<hr/>				
	Mean	S.D.		
Phase lag, pitch angle	$\delta_{y-\alpha}=-0.25T$	$\pm 0.067$		
Curvature half-wavelength	$\lambda_{\kappa}/2=0.427L$	$\pm 0.0422$		
Lateral body amplitude	$y_{0,11}=0.065L$	$\pm 0.0232$		
*See also Fig. 3.				
adj., adjusted.				
$T$ =tailbeat period, $L$ =body length.				
$P<0.05$ are significant and indicated as such in bold, $N=23$ .				
Means are given when no significant linear regression was found.				

contrasts between  $\omega$  categories revealed that  $EI$  increased from  $2\pi$  to  $4\pi$  and from  $4\pi$  to  $6\pi \text{ rad s}^{-1}$ ,  $C$  decreased at each level, and  $W$  increased from  $2\pi$  to  $4\pi \text{ rad s}^{-1}$  (Fig. 4). With changes in TRT, all five visco-elastic properties varied significantly; *a priori* contrasts (Table 5) between TRT categories revealed

that  $EI$  decreased when the notochordal core was isolated, the apparent Young's modulus  $E$ , increased when the axial muscles were removed from the notochord,  $C$  decreased when the skin was removed and when the notochordal core was isolated, and the resilience  $R$  decreased when the notochordal core was isolated. The interaction of  $\omega$  and TRT was significant for  $EI$ ,  $E$ ,  $C$  and  $W$ ; inspection of the graphical patterns (see Fig. 4) reveals that there is little effect of  $\omega$  on core  $EI$ ,  $E$  shows little or no  $\omega$  effect with the body intact and the skin removed, and  $C$  and  $W$  show little or no  $\omega$  effect with the core of the notochord. Finally, the compound factor of IND nested within TRT and  $\kappa$  was significant for all five variables; since this factor sequestered variance caused by differences between individual hagfish, it eliminates those effects, which are not of interest for the purposes of this study, from the responses of the other factors.

$EI$  of the intact body did not decrease significantly with the removal of the skin or the axial muscle. Even though the differences were not significant, the mean  $EI$  of the notochord whole body decreased by 25% compared to the mean  $EI$  of the whole body (values pooled across  $\omega$ ,  $\kappa$  and IND). Thus, conservatively, the notochord provides the body with 75% of its total  $EI$ . When the lateral musculature was removed,  $E$  increased significantly, by an order of magnitude from a mean of 0.38 to 4.97 MPa (values pooled across  $\omega$ ,  $\kappa$  and IND). The notochord has a high  $EI$ , in spite of a significantly reduced  $I$  (see Fig. 2D), because of an increased  $E$  relative to that of the whole body.

Flexural damping  $C$  decreased significantly when the skin was removed, implicating the subcutaneous sinus as a source of flexural damping; the mean (values pooled across  $\omega$ ,  $\kappa$  and IND) decreased 20% from 6.33 to 5.07 kg m<sup>3</sup> s<sup>-1</sup>. Since no significant decreases in  $C$  were detected with the removal of the lateral musculature, the notochord must be the primary source of the body's flexural damping, providing 80% of the total  $C$ . The damping function of the notochord is also supported by the lack of change in flexural work  $W$ , which is a function of  $C$  (see Equation 8) and resilience  $R$ , with the removal of the lateral musculature.

Flexural damping and stiffness were correlated. With

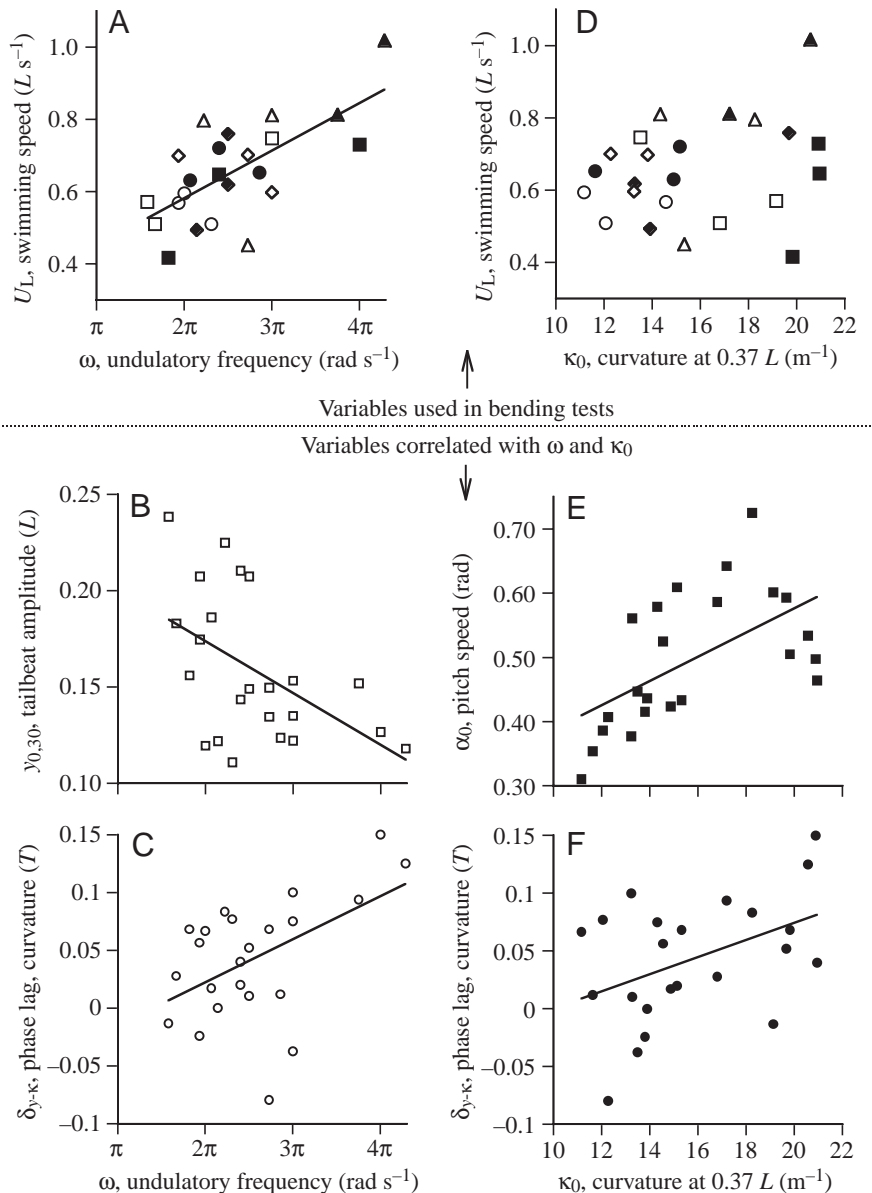


Fig. 3. Kinematic analysis of swimming. (A) Undulatory frequency  $\omega$  is the only significant ( $P < 0.05$ ) predictor of swimming speed,  $U_L$ , in a multivariate regression with individual hagfish treated as a random effect (see Table 2). Also,  $\omega$  is significantly correlated, as determined by univariate regression (see Table 3), with tailbeat amplitude  $y_{0,30}$  (B) and phase lag between heave and curvature at body point 11,  $\delta_{y-\kappa}$  (C). (D) The amplitude of the midline curvature at point 11 ( $0.37L$ ),  $\kappa_0$ , is not a significant predictor of  $U_L$ . It is, however, a significant predictor of pitch angle  $\alpha_0$  (E) and phase lag, curvature  $\delta_{y-\kappa}$  (F). Lines are significant regressions (see Tables 2, 3). Symbols in A and D indicate eight different individuals (total  $N=23$ ).

increasing  $C$ ,  $EI$  decreased rapidly (Fig. 5A) for all structural treatments. In contrast, with increasing damping moments, the stiffness moments increased linearly (Table 6; Fig. 5B) for all structural treatments. As  $\omega$  increased, the ratio of stiffness moments to damping moments increased linearly for the skin-off treatment but not for the others (Fig. 5C); the ratio derived by assuming frequency-independent values of  $EI$  and  $C$  decreased with increasing  $\omega$ .

**Discussion**

During dynamic bending that mimics the motion of steady swimming, the visco-elastic properties of the hagfish's intact body are dominated by those of the notochord (Fig. 4), which provides 75% of the body's flexural stiffness  $EI$ , and 80% of its flexural damping  $C$ . This conclusion is surprising for two reasons. (1) We expected that the passive visco-elastic properties of the lateral musculature would contribute

substantially to both  $EI$  and  $C$  because the musculature is responsible for the majority of the body's cross-sectional area (Fig. 2B). (2) The notochord occupies a position at or near the presumed neutral axis of bending and, hence, should have a disproportionately small contribution to  $EI$ , as predicted by the notochord's reduced second moment of area  $I$  (Fig. 2C). These expectations are violated (Fig. 5): the notochord compensates for its small  $I$  by having, relative to the whole

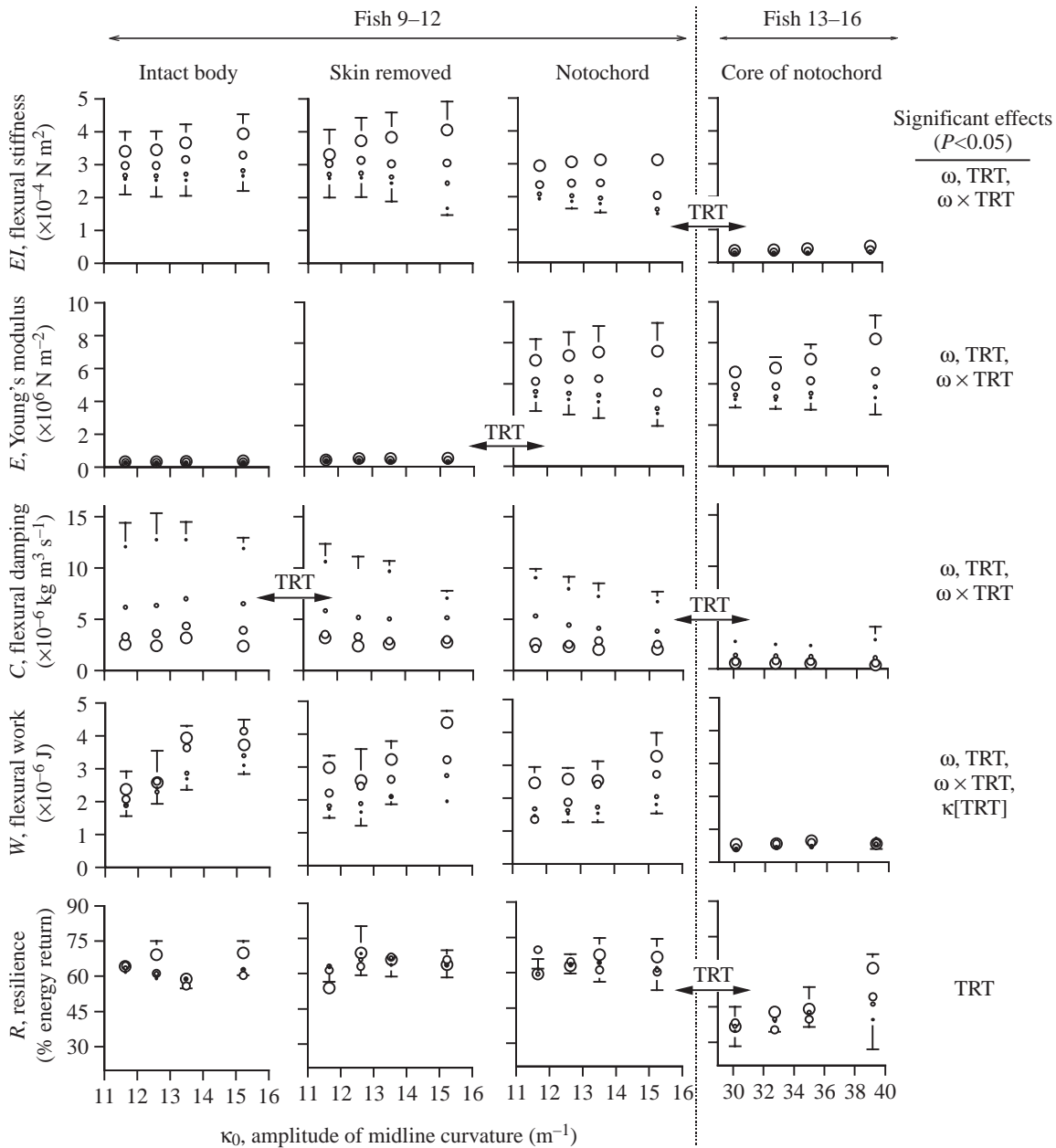


Fig. 4. Visco-elastic properties of the body axis (at  $0.37L$ ) of hagfish during dynamic bending. The diameter of the plotted circle is proportional to the experimental angular frequency  $\omega$  at  $\pi, 2\pi, 4\pi, 6\pi \text{ rad s}^{-1}$ . Statistically significant ( $P < 0.05$ ) overall differences for each property are listed in the far right-hand column (see Table 4); differences between treatments TRT (planned contrasts) are indicated by the labeled double-headed arrows between graphs (see Table 5). As indicated by the label for fish number, the notochord properties (penultimate right-hand column) were measured on different individuals, a condition necessitated by the isolation procedure and that accounted for use of a nested design (indicated as  $\kappa[\text{TRT}]$ , or 'curvature nested within treatment', when significance is indicated). Values of circles are means; error bars are  $\pm$  one standard error from pooling of individuals ( $N=4$ ).

body, a disproportionately large apparent Young's modulus  $E$  (Fig. 4).

The mechanical dominance of the notochord has four important implications, each of which is addressed in the following sections. (1) The frequency-dependent visco-elastic properties of the notochord interact dynamically to give it the capacity to amplify and stabilize undulatory swimming motions of the whole body (Figs 4, 5). This dynamic capacity has been omitted from computational models of swimmers with notochords, such as lamprey (Ekeberg, 1993; Carling et

al., 1998; Isjpeert et al., 1998, 1999a, 1999b) and amphibian tadpoles (Lui et al., 1996, 1997; Hoff and Wassersug, 2000), and its inclusion may enhance locomotor performance in next-generation simulations that couple internal and external forces. (2) The similarity in mechanical properties in notochords and intervertebral joints (Fig. 6) suggests a common structural and physicochemical basis. (3) Scenarios of the evolution of vertebral columns are informed by an understanding of the mechanical capacities of notochords during swimming (Koob and Long, 2000; McHenry, 2001). (4) Some of the unique

Table 4. Summary of F-values (Type III sums of squares) from nested ANOVAs performed separately on mechanical variables from bending hagfish bodies

Variable	$\omega$ (3,180)	TRT (3,60)	$\omega \times$ TRT (9,180)	$\kappa$ [TRT] (12,180)	IND[TRT, $\kappa$ ] (48,180)
$EI$	34.26 (< <b>0.0001</b> )	6.43 ( <b>0.001</b> )	10.77 (< <b>0.0001</b> )	0.06 (1.00)	31.57 (< <b>0.0001</b> )
$E$	0.19 (0.902)	11.98 (< <b>0.0001</b> )	37.92 (< <b>0.0001</b> )	0.13 (0.999)	42.52 (< <b>0.0001</b> )
$C$	239.70 (< <b>0.0001</b> )	34.03 (< <b>0.0001</b> )	25.30 (< <b>0.0001</b> )	0.29 (0.989)	6.71 (< <b>0.0001</b> )
$W$	8.04 (< <b>0.0001</b> )	3.54 ( <b>0.019</b> )	5.18 ( <b>0.0001</b> )	1.76 (0.082)	8.27 (< <b>0.0001</b> )
$R$	2.17 (0.093)	7.74 ( <b>0.0002</b> )	1.39 (0.195)	0.37 (0.967)	12.48 (< <b>0.0001</b> )

$P$ -values are indicated in parentheses;  $P < 0.05$  is significant and indicated as such in bold,  $N = 256$ .

Degrees of freedom (model, error) are given in parentheses below each factor.

$\kappa$ [TRT] is ' $\kappa$  nested within TRT', and represents the combined effects of  $\kappa$  and the  $\kappa \times$  TRT interaction (see Zar, 1996); analogous reasoning is used for the compound nested term, this nested term IND[TRT, $\kappa$ ]. For experimental justification, see Materials and methods.

See List of symbols for definitions of variables and units.

Table 5. Planned a priori contrasts within the factors of angular frequency  $\omega$ , and structural treatment

Variable	Angular frequency $\omega$			Structural treatment		
	$\pi$ versus $2\pi$	$2\pi$ versus $4\pi$	$4\pi$ versus $6\pi$	Whole versus skin removed	Skin off versus notochord	Notochord versus core
$EI$	-1.30 (0.196)	-3.35 ( <b>0.001</b> )	-4.62 (< <b>0.0001</b> )	0.42 (0.679)	0.73 (0.466)	2.83 ( <b>0.007</b> )
$E$	-0.09 (0.925)	-0.25 (0.804)	-0.35 (0.727)	-0.07 (0.944)	4.31 (< <b>0.0001</b> )	0.20 (0.839)
$C$	14.78 (< <b>0.0001</b> )	2.70 (< <b>0.0001</b> )	2.96 ( <b>0.004</b> )	2.35 ( <b>0.022</b> )	1.52 (0.519)	5.82 (< <b>0.0001</b> )
$W$	-0.49 (0.622)	-3.07 ( <b>0.003</b> )	-2.71 (0.787)	0.41 (0.681)	0.65 (0.519)	1.95 (0.056)
$R$	-0.39 (0.701)	0.50 (0.621)	-2.24 ( <b>0.026</b> )	0.22 (0.828)	-0.19 (0.850)	3.98 ( <b>0.0002</b> )

$P$ -values are indicated in parentheses for each value of  $t$ ;  $P < 0.05$  are significant and indicated as such in bold,  $N = 256$ .

See List of symbols for definitions of variables and units.

Table 6. Regression equations relating stiffness to damping

Treatment	$EI$ versus $C$	$EI\kappa_0$ versus $C\kappa_0\omega$	$EI/C\omega$ versus $\omega$ , empirical	$EI/C\omega$ versus $\omega$ , theoretical
Intact	$EI = 357.0C^{-3.86}$ $r^2 = 0.80$	$EI\kappa_0 = 6.51C\kappa_0\omega + 0.27$ $r^2 = 0.80$ ; $P < 0.0001$	$EI/C\omega = 0.042\omega + 6.37$ $r^2 = 0.55$ ; $P = 0.257$	$EI/C\omega = 20.8\omega^{-1.0}$ $r^2 = 1.00$
Skin off	$EI = 29.3C^{-1.77}$ $r^2 = 0.56$	$EI\kappa_0 = 6.11C\kappa_0\omega + 0.40$ $r^2 = 0.68$ ; $P < 0.0001$	$EI/C\omega = -0.049\omega + 8.29$ $r^2 = 0.96$ ; $P = 0.020$	$EI/C\omega = 25.8\omega^{-1.0}$ $r^2 = 1.00$
Notochord	$EI = 14.18.0C^{-1.69}$ $r^2 = 0.59$	$EI\kappa_0 = 6.15C\kappa_0\omega + 0.78$ $r^2 = 0.77$ ; $P < 0.0001$	$EI/C\omega = 0.007\omega + 7.13$ $r^2 = 0.07$ ; $P = 0.729$	$EI/C\omega = 22.9\omega^{-1.0}$ $r^2 = 1.00$
Core	$EI = 0.03C^{-3.03}$ $r^2 = 0.80$	$EI\kappa_0 = 2.58C\kappa_0\omega + 0.39$ $r^2 = 0.11$ ; $P = 0.207$	$EI/C\omega = 0.066\omega + 3.26$ $r^2 = 0.87$ ; $P = 0.059$	$EI/C\omega = 10.7\omega^{-1.0}$ $r^2 = 1.00$

$P < 0.05$  is significant and indicated as such in bold,  $N = 16$  for each regression.

Note that  $P$ -values for regressions using power functions are not normally given.

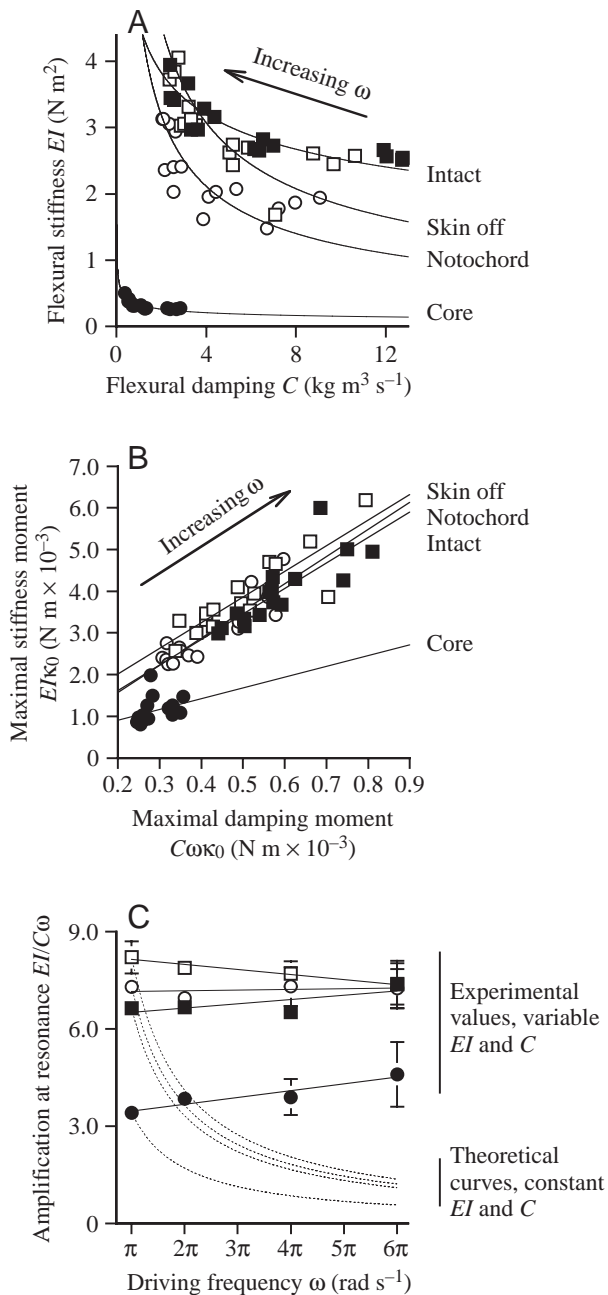


Fig. 5. Coupling of stiffness and damping in the body and notochord of hagfish during dynamic bending. (A) As flexural damping  $C$  increases, flexural stiffness  $EI$  decreases. Parameterized within the power curves (see Table 6) is driving frequency  $\omega$ . (B) The maximal bending moments produced by stiffness and damping are directly and linearly proportional (see Table 6 for equations). (C) Experimentally derived values for the ratio of stiffness moments to damping moments change minimally, compared to theoretical ratios assuming constant  $EI$  and  $C$  (dotted lines), as  $\omega$  changes (see Table 6). If  $\omega$  is equal to the resonance frequency, the ratio is a special case of Equation 1, and estimates the maximum possible amplification of internal stresses. Filled squares, the 'intact' structural treatment category; open squares, the 'skin removed' category; open circles, the 'notochord' category; filled circles, the 'core' category.

kinematic features of hagfish swimming may be caused by the mechanical properties of the notochord.

#### Mechanical capacities of the notochord during steady swimming

The visco-elastic properties of the notochord give it the capacity to function as both a motion stabilizer and a mechanical power amplifier. While springs acting as force transmitters in oscillating propulsive systems reduce energy costs by reducing negative work, they may cause unstable dynamics (Harper et al., 1998). Dynamic instability may be controlled actively, by sensory-muscular control, or passively, using the system's constitutive mechanical properties (Harper et al., 1998). Passive stability is preferable in animal locomotion in certain situations, because it provides faster and simpler mechanical feedback and response (Dickinson et al., 2000).

In hagfish, evidence for passive dynamic stability comes from the ratio of stiffness to damping moments, a special case of Equation 1 that assumes that the system is always bending at its resonance frequency (see Introduction). While operating at resonance provides energy savings to swimming animals (DeMont, 1990; Oxner et al., 1993; for reviews, see Long and Nipper, 1996; Pabst, 1998), the amplification of bending or stresses that produces those savings may lead to catastrophic failure if they are undamped (Denny, 1988). Thus, we examined the ratio of stiffness moments and damping moments at all observed undulatory frequencies to determine if there might be any situation in which resonant swimming might lead to break-away bending. Unexpectedly,  $EI$  and  $C$  of the hagfish notochord adjust with changes in  $\omega$  (Fig. 5A) to produce a nearly constant amplification ratio of seven (Fig. 5C). Thus, the notochord would amplify force or curvature and, at the same time, limit that amplification if hagfish were swimming with an  $\omega$  at or near their resonance frequency. In other words, the visco-elastic properties of the notochord provide the body with a nearly constant dynamic stability over a wide range of swimming speeds.

Hagfish could take advantage of their dynamic passive stability by using their muscles to adjust the stiffness of their body to match the resonance frequency to any  $\omega$  at which they are swimming. Such active tuning was first suggested by Blight (1977), and adjustable body stiffness has been shown to affect swimming performance in physical sunfish models (McHenry et al., 1995) and computational simulations of sunfish (Long et al., 2002) and lamprey (Ijspeert et al., 1998). Myomeric muscles of eel *Anguilla rostrata* have the capacity to increase the body's  $EI$  and  $C$  by a factor of three and seven, respectively (Long, 1998). Taken in combination, these results suggest that hagfish may have the capacity to engage in variable resonance swimming.

#### Structural and physicochemical basis of mechanical properties

It is surprising that the notochord, a hydrostatic, fiber-wound cylinder, could have the apparent material stiffness  $E$  and size-

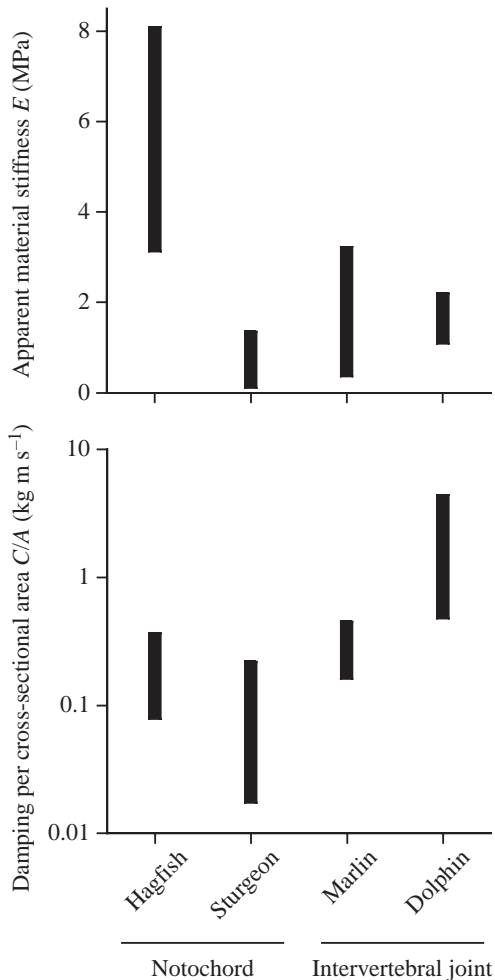


Fig. 6. The range of visco-elastic properties of different axial skeletons subjected to sinusoidal bending. The notochords of hagfish ( $N=4$ ) have apparent material stiffnesses (or Young's modulus)  $E$ , greater than that of the notochord ( $N=1$ ) of white sturgeon *Acipenser transmontanus* (Long, 1995), the intervertebral joints ( $N=6$ ) of blue marlin *Makaira nigricans* (Long, 1992) and the intervertebral joints ( $N=3$ ) of saddleback dolphin *Delphinus delphis* (Long et al., 1997). Flexural damping  $C$  is normalized per cross-sectional area  $A$  of the notochord or intervertebral joint (note units of momentum); the notochord of hagfish has a range of values overlapping the range for sturgeon and marlin. For each species, the range of mean values are given (black bars) from dynamic cantilevered bending tests conducted at physiologically relevant curvatures and driving frequencies. The ranges include regional variation, when measured.

independent damping  $C/A$  comparable to the intervertebral joints in a segmented, bony vertebral column in a fish and cetacean (Fig. 6). For comparison, a motion segment of the intact human vertebral column, including the intervertebral disc and articular processes of the neural spine, has a storage modulus  $G'$  (roughly equivalent to  $E$ , depending on loading conditions) of 45 MPa (for a review, see Iatridis et al., 1996). The  $G'$  of the isolated nucleus pulposus and annulus fibrosus are much lower, ranging from 0.01 MPa (Iatridis et al., 1996) to 0.20 MPa (Iatridis et al., 1999) in the former and

0.007–0.020 MPa (Iatridis et al., 1997) in the latter. The basis for the correspondence in aquatic species may derive in part from the similarity between physicochemical properties of the notochord core and those of intervertebral discs and joints: the mechanical properties of both systems appear to be based on hydrostatic mechanisms (for reviews, see Wainwright, 1988; Hukins and Meakin, 2000; Koob and Long, 2000).

Physicochemical measurements coupled with mechanical tests provide a preliminary basis for understanding the mechanical properties of the notochord. Bulk free-swelling tests on isolated segments have established that the notochord's core is osmotically active: it swells in solutions with ionic strength below that *in vivo*, and shrinks in higher ionic strength solutions (Koob et al., 1994). The flexural stiffness  $EI$  and apparent material stiffness  $E$  of the notochord are inversely proportional to the osmolarity of the bathing solution (Sinwell et al., 1999). These observations suggest that the core of the notochord exerts a swelling pressure on the constraining fibrous sheath, imparting the high, hydrostatically controlled material stiffness.

Unfortunately, far too little is known about intervertebral discs and joints in non-mammalian species for a satisfactory comparison. Nevertheless, several common features should be mentioned. Unconstricted notochords in sturgeon and lungfish are organized essentially the same as the hagfish notochord, and display similarities with respect to cell morphology in having large vacuoles bounded by intermediate filaments (Schmitz, 1998). The yellow perch's intervertebral joint, which is derived from the notochord, is also made up in large part of interconnected cells with large vacuoles (Schmitz, 1995). The situation is different in mammalian intervertebral joints. The core of these joints, the nucleus pulposus, is predominantly extracellular matrix (for a review, see Urban et al., 2000).

#### *Evolution of the function of the notochord and vertebrae*

Adults in all the extant chordate clades can be found that retain an unsegmented notochord associated with axial musculature driving undulatory flexures. Within Urochordata, the appendicularians retain a notochord in a muscular tail used for locomotion or feeding (Nishino and Satoh, 2001). In Cephalochordata (lancelets) and Myxiniiformes (hagfishes), free-swimming and burrowing adults retain a notochord (Gee, 1996). In vertebrates, the unsegmented notochord has been retained with the addition of neural and hemal arches of cartilage or bone in lamprey, some shark, lungfish, sturgeon and paddlefish (Goodrich, 1930). Since many other metazoans without notochords also engage in undulatory swimming (Clark, 1964), the evolution of the notochord was not a prerequisite.

Given this comparative information, the unsegmented notochord of hagfishes is not degenerate; the unsegmented notochord engaged in undulatory motion is the ancestral character state of the axial skeleton in Craniata (hagfishes and vertebrates). This evolutionary direction has received additional support from the phylogenetic placement of the Lower Cambrian hagfish-like fossil *Haikouella*, which possesses an unsegmented notochord, as a clade between

cephalochordates and myxiniiformes (Holland and Chen, 2001). We argue that by examining the mechanics of the notochord of the marine hagfish, we investigate an axial skeletal system that is likely to have retained functional features common to the stem lineage of Chordata. By contrast, we would not argue the same if we had chosen to examine *Branchiostoma*, a lancelet whose notochord appears to have derived features such as intrinsic paramyosin that actively alter flexural stiffness (Webb, 1973).

Within Craniata (hagfishes and vertebrates), the notochord evolved segmentation in the form of vertebral centra (Gee, 1996). The number of vertebrae is inversely proportional to the magnitude of body curvature in fast-starting fish (Brainerd and Patek, 1998) and steadily swimming undulatory vertebrates (Long and Nipper, 1996). Thus vertebrae may stiffen the body. An alternative hypothesis, and one that we can test with our data on hagfish notochords, is that the apparent increased body stiffness comes not from the vertebrae *per se* but from increases in the material stiffness and damping of the connective tissues of the invertebral joints. Our data do not support this alternative (Fig. 6). Instead, the apparent material stiffness,  $E$ , and the damping per cross-sectional area,  $C/A$ , are nearly equal in notochords and intervertebral joints. Vertebrae, being much stiffer, mineralized elements, restrict bending to the joints. Thus for a given amount of body curvature, the internal strain and stress on any section of notochordal tissue would be much less than that on the tissues of an intervertebral joint.

#### Midline kinematics of swimming hagfish

To our knowledge (see also Vogel and Gemballa, 2000), this is the first quantitative analysis of the undulatory swimming motions of hagfish (for qualitative observations, see Adams, 1960). While our original intent in videotaping steadily swimming hagfish was to determine physiologically relevant ranges for  $\omega$  and  $\kappa$  in the bending experiments, the kinematic results are of interest in their own right (Fig. 3). At the swimming speeds measured here, ranging from a speed  $U_L$  of 0.4 to  $1.0 L s^{-1}$ , we find that while undulatory frequency  $\omega$  increases linearly with respect to  $U_L$ , tailbeat amplitude  $y_{0,30}$  decreases linearly with respect to  $\omega$  (Fig. 3A,B). This is an unexpected result. From undulatory teleosts, we expected that  $\omega$  and  $y_{0,30}$  would increase in concert at speeds below  $5 L s^{-1}$  (Bainbridge, 1958, 1963), or that  $y_{0,30}$  would remain constant (Webb et al., 1984; for a review, see Videler, 1993). This decrease in  $y_{0,30}$  may be due, in part, to the increasing stiffness  $EI$  of the notochord with increasing  $\omega$  (Fig. 5). Furthermore, since the squares of  $\omega$  and  $y_{0,30}$  are proportional to hydromechanical power output (Wu, 1977; Webb et al., 1984), in order to swim faster a decrease in  $y_{0,30}$  must be compensated for by either a disproportionately large increase in  $\omega$  or an increase in propulsive efficiency. Since  $\omega$  nearly doubles over the observed ranged of speeds and  $y_{0,30}$  decreases by nearly half (Fig. 3), the changes in hydromechanical power should cancel out while notochord and body stiffness increase. Clearly, more work is required to fully understand the mechanics of steady swimming in hagfish.

#### List of symbols used

$A$	cross-sectional area ( $m^2$ )
$C$	flexural damping ( $kg\ m^3\ s^{-1}$ )
$E$	Young's modulus, apparent material stiffness (MPa)
$EI$	flexural stiffness ( $N\ m^2$ )
$G'$	storage modulus (MPa)
$I$	moment of inertia ( $m^4$ )
$I_a$ ,	area moment of inertia ( $m^4$ )
$I_m$	mass moment of inertia ( $kg\ m^2$ )
$L$	normalized body length (%)
$L_b$	body length (m)
$l$	section length (m)
$M$	bending moment (N m)
$M_0$	amplitude of bending moment (N m)
$r$	cross-sectional radius (m)
$R$	resilience (elastic energy return) (%)
$t$	time (s)
$T$	normalized tailbeat period
$U$	swimming speed ( $m\ s^{-1}$ )
$U_L$	length-specific swimming speed ( $L\ s^{-1}$ )
$W$	flexural work, net for one cycle (J)
$x$	position along dimension of forward body motion (m)
$y$	position along dimension of lateral body motion (m)
$y_{0,11}$	amplitude of lateral displacement at midline point 11 $L$
$y_{0,30}$	amplitude of lateral displacement at midline point 30 $L$
$\alpha$	pitch angle (rad)
$\alpha_0$	amplitude of pitch angle (rad)
$\theta$	midline flexion (rad)
$\theta_0$	amplitude of midline flexion (rad)
$\delta$	phase lag (rad)
$\delta_{y-\alpha}$	phase lag from $y_{0,11}$ to $\alpha_0$ ( $T$ )
$\delta_{y-\beta}$	phase lag from $y_{0,11}$ to $\beta_0$ ( $T$ )
$\kappa$	midline curvature ( $m^{-1}$ )
$\kappa_0$	amplitude of midline curvature ( $m^{-1}$ )
$\lambda_{\kappa}/2$	curvature half-wave length along axis ( $L$ )
$\omega$	undulatory frequency ( $rad\ s^{-1}$ )

This work was supported by grants from the Office of Naval Research to J.H.L. (ONR no. N00014-997-1-0292) and Shriners of North America to T.J.K. (no. 8610). B.J.S. was supported by a Fellowship from the Undergraduate Research Summer Institute of Vassar College. The authors thank Matt McHenry, Wyatt Korff, Robert Suter, Ben Johns, and two anonymous reviewers for their constructive comments on the manuscript. We also thank the staff of the Mount Desert Island Biological Laboratory for their patience and support.

#### References

- Adams, H. (1960). Different types of body movement in the hagfish, *Myxine glutinosa*. *Nature* **188**, 595-596.
- Bainbridge, R. (1958). The speed of swimming of fish as related to size and to the frequency and amplitude of the tail beat. *J. Exp. Biol.* **35**, 109-133.
- Bainbridge, R. (1963). Caudal fin and body movement in the propulsion of some fish. *J. Exp. Biol.* **40**, 23-56.

- Blight, A. R.** (1977). The muscular control of vertebrate swimming movements. *Biol. Rev.* **52**, 181-218.
- Brainerd, E. L. and Patek, S. N.** (1998). Vertebral column morphology, c-start curvature, and the evolution of mechanical defenses in tetraodontiform fishes. *Copeia* **1998**, 971-984.
- Carling, J. C., Williams, T. L. and Bowtell, G.** (1998). Self-propelled anguilliform swimming: simultaneous solution of the two-dimensional Navier-Stokes equations and Newton's laws of motion. *J. Exp. Biol.* **201**, 3143-3166.
- Clark, R. B.** (1964). *Dynamics in Metazoan Evolution: the Origin of the Coelom and Segments*. Oxford: Clarendon Press.
- Cole, F. J.** (1905). A monograph on the general morphology of the myxinoïd fishes, based on a study of *Myxine*. Part 1. The anatomy of the skeleton. *Trans. R. Soc. Edinburgh* **XLI**, 749-788.
- DeMont, M. E.** (1990). Tuned oscillations in the swimming scallop *Pecten maximus*. *Can. J. Zool.* **78**, 786-791.
- Den Hartog, J. P.** (1956). *Mechanical Vibrations*, 4th edition (reprinted, 1985). USA: Dover Publications.
- Denny, M. W.** (1988). *Biology and Mechanics of the Wave-Swept Environment*. Princeton, NJ, USA: Princeton University Press.
- Dickinson, M. H., Farley, C. T., Full, R. J., Koehl, M. A. R., Kram, R. and Lehman, S.** (2000). How animals move: an integrative view. *Science* **288**, 100-106.
- Ekeberg, O.** (1993). A combined neuronal and mechanical model of fish swimming. *Biol. Cybernet.* **69**, 363-374.
- Forster, M. E.** (1997). The blood sinus system of hagfish: its significance in a low-pressure circulation. *Comp. Biochem. Physiol. A* **116**, 239-244.
- Gee, H.** (1996). *Before the Backbone: Views on the Origins of the Vertebrates*. London, UK: Chapman and Hall.
- Goodrich, E.** (1930). *Studies on the Structure and Development of Vertebrates*. London: Macmillan.
- Harper, K. A., Berkemeier, M. D. and Grace, S.** (1998). Modeling the dynamics of spring-driven, oscillating-foil propulsion. *IEEE J. Oceanic Eng.* **23**, 285-296.
- Hoff, K. V. S. and Wassersug, R. J.** (2000). Tadpole locomotion: Axial movement and tail functions in a largely vertebraless vertebrate. *Am. Zool.* **40**, 62-76.
- Holland, N. D. and Chen, J.** (2001). Origin and early evolution of the vertebrates: new insights from advances in molecular biology, anatomy, and paleontology. *BioEssays* **23**, 142-151.
- Hukins, D. W. L. and Meakin, J. R.** (2000). Relationship between structure and mechanical function of the tissues of the intervertebral joint. *Amer. Zool.* **40**, 42-52.
- Iatridis, J. C., Kumar, S., Foster, R. J. and Mow, V. C.** (1999). Shear mechanical properties of human lumbar annulus fibrosus. *J. Orth. Res.* **17**, 732-737.
- Iatridis, J. C., Setton, L. A., Weidenbaum, M. and Mow, V. C.** (1997). Visco-elastic behaviors of the human lumbar nucleus pulposus in shear. *J. Biomech.* **30**, 1005-1013.
- Iatridis, J. C., Weidenbaum, M., Setton, L. A. and Mow, V. C.** (1996). Is the nucleus pulposus a solid or fluid? Mechanical behaviors of the nucleus pulposus of the human intervertebral disc. *Spine* **21**, 1174-1184.
- Ijspeert, A. J., Hallam, J. and Willshaw, D.** (1998). From lampreys to salamanders: evolving neural controllers for swimming and walking. In *From Animals to Animats 5: Proceedings of the Fifth International Conference on Simulation of Adaptive Behavior* (ed. R. Pfeifer, B. Blumberg, J.-A. Meyer and S. W. Wilson), pp. 390-399. Cambridge, MA, USA: MIT Press.
- Ijspeert, A. J., Hallam, J. and Willshaw, D.** (1999a). Evolving swimming controllers for a simulated lamprey with inspiration from neurobiology. *Adapt. Behav.* **7**, 151-172.
- Ijspeert, A. J. and Kodjabachian, J.** (1999b). Evolution and development of a central pattern generator for the swimming of a lamprey. *Artificial Life* **5**, 247-269.
- Jayne, B. C. and Lauder, G. V.** (1993). Red and white muscle activity and kinematics of the escape response of the bluegill sunfish during swimming. *Comp. Physiol. A* **173**, 495-508.
- Kielstein, J. T., Stolte, H. and Koob, T. J.** (1996). Biomechanical properties of hagfish (*Myxine glutinosa*) notochord. *The Bulletin, Mt. Desert Isl. Biol. Lab.* **35**, 105-107.
- Koob, T. J., Kielstein, J. T., Koob-Emunds, M. and Stolte, H.** (1994). Physicochemical properties and proteoglycans of the hagfish (*Myxine glutinosa*) notochord. *The Bulletin, Mt. Desert Isl. Biol. Lab.* **33**, 5-8.
- Koob, T. J. and Long, J. H., Jr** (2000). The vertebrate body axis: evolution and mechanical function. *Am. Zool.* **40**, 1-18.
- Long, J. H., Jr** (1992). Stiffness and damping forces in the intervertebral joints of blue marlin (*Makaira nigricans*). *J. Exp. Biol.* **162**, 131-155.
- Long, J. H., Jr** (1995). Morphology, mechanics, and locomotion: the relation between the notochord and swimming motions in sturgeon. *Env. Biol. Fishes* **44**, 199-211.
- Long, J. H., Jr** (1998). Muscles, elastic energy, and the dynamics of body stiffness in swimming eels. *Am. Zool.* **38**, 771-792.
- Long, J. H., Jr, Adcock, B. and Root, R. G.** (2002). Force transmission via axial tendons in undulating fish: a dynamic analysis. *Comp. Biochem. Physiol.* (in press).
- Long, J. H., Jr, Koob-Emunds, M. and Koob, T. J.** (1998). Does the notochord matter? Bending mechanics of hagfish (*Myxine glutinosa*). *The Bulletin, MDI Biol. Lab.* **37**, 114-116.
- Long, J. H., Jr and Nipper, K. S.** (1996). The importance of body stiffness in undulatory propulsion. *Am. Zool.* **36**, 678-694.
- Long, J. H., Jr, Pabst, D. A., Shepherd, W. R. and McLellan, W. A.** (1997). Locomotor design of dolphin vertebral columns: bending mechanics and morphology of *Delphinus delphis*. *J. Exp. Biol.* **200**, 65-81.
- Lui, H., Wassersug, R. J. and Kawachi, K.** (1996). A computational fluid dynamics study of tadpole swimming. *J. Exp. Biol.* **199**, 1245-1260.
- Lui, H., Wassersug, R. J. and Kawachi, K.** (1997). The three-dimensional hydrodynamics of tadpole locomotion. *J. Exp. Biol.* **200**, 2807-2819.
- Martini, F. H., Lesser, M. P. and Heiser, J. B.** (1997). Ecology of the hagfish, *Myxine glutinosa* L. in the Gulf of Maine. II. Potential impact on benthic communities and commercial fisheries. *J. Exp. Mar. Biol. Ecol.* **214**, 97-106.
- McHenry, M. J.** (2001). Mechanisms of helical swimming: asymmetries in the morphology, movement and mechanics of larvae of the ascidian *Distaplia occidentalis*. *J. Exp. Biol.* **204**, 2959-2973.
- McHenry, M. J., Pell, C. A. and Long, J. H., Jr** (1995). Mechanical control of swimming speed: stiffness and axial wave form in an undulatory fish model. *J. Exp. Biol.* **198**, 2293-2305.
- Nishino, A. and Satoh, N.** (2001). The simple tail of chordates: phylogenetic significance of appendicularians. *Genesis* **29**, 36-45.
- Oxner, W. M., Quinn, J. and DeMont, E. M.** (1993). A mathematical model of body kinematics in swimming tadpoles. *Can. J. Zool.* **71**, 407-413.
- Pabst, D. A.** (1998). Spring in swimming animals. *Am. Zool.* **36**, 723-735.
- Riegel, J. A.** (1978). Factors affecting glomerular function in the Pacific hagfish *Eptatretus stouti* (Lockington). *J. Exp. Biol.* **73**, 261-277.
- Schmitz, R. J.** (1995). Ultrastructure and function of cellular components of the intercentral joint in the percoid vertebral column. *J. Morph.* **226**, 1-24.
- Schmitz, R. J.** (1998). Comparative ultrastructure of the cellular components of the uncontracted notochord in the sturgeon and the lungfish. *J. Morph.* **236**, 75-104.
- Sinwell, B. J., Czuwala, P. J., Long, J. H., Jr, Koob-Emunds, M. and Koob, T. J.** (1999). Bending mechanics of the hagfish (*Myxine glutinosa*) notochord under different osmotic treatments. *The Bulletin, Mt. Desert Isl. Biol. Lab.* **38**, 94-96.
- Urban, J. P. G., Roberts, S. and Ralphs, J. R.** (2000). The nucleus of the intervertebral disc from development to degeneration. *Am. Zool.* **40**, 53-61.
- Videler, J. J.** (1993). *Fish Swimming*. London: Chapman and Hall.
- Vogel, F. and Gemballa, S.** (2000). Locomotory design of 'cyclostome' fishes: spatial arrangement and architecture of myosepta and lamellae. *Acta Zool.* **81**, 267-283.
- Vogel, S.** (1994). *Life in Moving Fluids*. 2nd Edition. Princeton, NJ, USA: Princeton University Press.
- Wainwright, S. A.** (1988). *Axis and Circumference: the Cylindrical Shape of Plants and Animals*. Cambridge, MA, USA: Harvard University Press.
- Wainwright, S. A., Biggs, W. D., Currey, J. D. and Gosline, J. M.** (1976). *Mechanical Design in Organisms*. New York: John Wiley and Sons.
- Webb, P. W., Kosteki, P. T. and Stevens, E. D.** (1984). The effect of size and swimming speed on locomotor kinematics of rainbow trout. *J. Exp. Biol.* **109**, 77-95.
- Webb, J. E.** (1973). The role of the notochord in forward and reverse swimming and burrowing in the amphioxus *Branchiostoma lanceolatum*. *J. Zool. Lond.* **170**, 325-338.
- Welsch, U., Chiba, A. and Honma, Y.** (1998). The notochord. In *The Biology of Hagfishes* (ed. J. Jørgensen, J. P. Lomholt, R. Weber and H. Malte), pp. 145-149. London: Chapman and Hall.
- Wu, T. Y.** (1977). Introduction to the scaling of aquatic animal locomotion. In *Scale Effects in Animal Locomotion* (ed. T. J. Pedley), pp. 203-232. New York: Academic Press.
- Zar, J. H.** (1996). *Biostatistical Analysis*. Upper Saddle River, NJ, USA: Prentice-Hall.